LETTER

https://doi.org/10.1038/s41586-018-0156-5

Prevalent lightning sferics at 600 megahertz near Jupiter's poles

Shannon Brown[1]*, Michael Janssen[1], Virgil Adumitroaie[1], Sushil Atreya[2], Scott Bolton[3], Samuel Gulkis[1], Andrew Ingersoll[4], Steven Levin[1], Cheng Li[4], Liming Li[5], Jonathan Lunine[6], Sidharth Misra[1], Glenn Orton[1], Paul Steffes[7], Fachreddin Tabataba-Vakili[4], Ivana Kolmašová[8,9], Masafumi Imai[10], Ondřej Santolík[8,9], William Kurth[10], George Hospodarsky[10], Donald Gurnett[10] & John Connerney[11]

Lightning has been detected on Jupiter by all visiting spacecraft through night-side optical imaging and whistler (lightning-generated radio waves) signatures[1–6]. Jovian lightning is thought to be generated in the mixed-phase (liquid–ice) region of convective water clouds through a charge-separation process between condensed liquid water and water-ice particles, similar to that of terrestrial (cloud-to-cloud) lightning[7–9]. Unlike terrestrial lightning, which emits broadly over the radio spectrum up to gigahertz frequencies[10,11], lightning on Jupiter has been detected only at kilohertz frequencies, despite a search for signals in the megahertz range[12]. Strong ionospheric attenuation or a lightning discharge much slower than that on Earth have been suggested as possible explanations for this discrepancy[13,14]. Here we report observations of Jovian lightning sferics (broadband electromagnetic impulses) at 600 megahertz from the Microwave Radiometer[15] onboard the Juno spacecraft. These detections imply that Jovian lightning discharges are not distinct from terrestrial lightning, as previously thought. In the first eight orbits of Juno, we detected 377 lightning sferics from pole to pole. We found lightning to be prevalent in the polar regions, absent near the equator, and most frequent in the northern hemisphere, at latitudes higher than 40 degrees north. Because the distribution of lightning is a proxy for moist convective activity, which is thought to be an important source of outward energy transport from the interior of the planet[16,17], increased convection towards the poles could indicate an outward internal heat flux that is preferentially weighted towards the poles[9,16,18]. The distribution of moist convection is important for understanding the composition, general circulation and energy transport on Jupiter.

Terrestrial radio emission from lightning peaks near 1–10 kHz and falls off rapidly with the frequency f, approximately as f^{-4}, above about 10 MHz[10,11]. Radio emission from lightning is detectable from a spacecraft at kilohertz frequencies in the form of whistlers (lightning-generated radio waves distorted into a decreasing tone by their passage through the plasma environment of the planet), which propagate from the source to the spacecraft along magnetic field lines, and at megahertz frequencies as sferics, which propagate directly from the source to the spacecraft. On Jupiter, whistlers were previously detected by the Voyager plasma wave receiver[19], but no high-frequency (10–40 MHz) sferic signals were observed by the companion planetary radio-astronomy receiver[20]. The Galileo probe also failed to detect high-frequency sferics[1,12]. One explanation for the absence of such signals is attenuation from low-altitude ionospheric layers[14]. However, such layers would also strongly attenuate emission at kilohertz frequencies. Therefore, a slow-discharge model with weak emission above 10 MHz has been proposed as an alternative explanation[13]. The closest approach of the Juno spacecraft to Jupiter is nearly 50 times greater than that of Voyager (up to 30 dB greater signal strength), and ionospheric attenuation, which decreases as f^{-2}, is not a contributor at 600 MHz, which is the lowest-frequency channel of the Juno microwave radiometer (MWR). On the basis of modelled and measured data[21], the electron density in the Jovian ionosphere is orders of magnitude lower than that required to generate even a minimally detectable ionospheric opacity at 600 MHz. Additionally, the observed variation of the MWR antenna temperature with emission angle on the planet is consistent with emission only from the deep atmosphere over all latitudes, and there is no evidence of an ionospheric contribution. The only exception is one localized spot over the portion of the aurora corresponding to the Io flux tube.

Lightning detection reveals areas of active moist convection in water clouds on Jupiter[5,7,8]. Our current understanding of the global distribution of lightning on Jupiter draws from limited surveys, giving an incomplete picture of the spatial distribution and frequency of moist convection. From the vantage point of Jupiter's polar orbit, the Juno observations provide new insights into the latitudinal distribution of lightning and moist convection from pole to pole. Juno is in a highly elliptical, 53-day polar orbit around Jupiter. The spacecraft is spinning at two revolutions per minute, with a spin vector roughly perpendicular to the orbit plane. The Juno MWR instrument was designed to probe thermal emission from the Jovian atmosphere well below the water-cloud region (at least 100 bar; 1 bar = 10^5 Pa) and thus place constraints on the deep water abundance of the planet's atmosphere. The instrument measures radiation in six microwave bands from 600 MHz to 22 GHz (1.3–50 cm)[15]. The two lowest-frequency channels (600 MHz and 1.26 GHz) have a Gaussian antenna pattern with a half-power width of 20°, which is scanned across the planet by the spacecraft spin.

The MWR continuously samples during Juno's orbit, integrating each radiance measurement for 0.1 s. Single positive outliers above the background atmospheric emission were observed in the time series of the 600-MHz measurement only while observing Jupiter. After eliminating all other plausible explanations for the source of these outliers, including instrument artefacts and other sources of non-thermal emission, we attribute them to lightning sferics. The lightning emission is extracted from the background signal by applying a low-pass filter to the radiometer's time series and selecting positive outliers that are six standard deviations above the noise (>5 K in antenna temperature). This yields a total of 377 detections at 600 MHz through the first eight (out of the 32 planned) orbits of Juno. Each detection represents the sum of all discharges that occurred within the antenna field of view during the 0.1-s integration period. Of these, 10 MWR detections were found to be coincident in time and location with lightning whistlers detected by the Waves instrument[22], further supporting lightning as the source of the

[1]Jet Propulsion Laboratory, California Institute of Technology, Pasadena, CA, USA. [2]Climate and Space Sciences and Engineering, University of Michigan, Ann Arbor, MI, USA. [3]Southwest Research Institute, San Antonio, TX, USA. [4]California Institute of Technology, Pasadena, CA, USA. [5]Department of Physics, University of Houston, Houston, TX, USA. [6]Department of Astronomy, Cornell University, Ithaca, NY, USA. [7]School of Electrical and Computer Engineering, Georgia Institute of Technology, Atlanta, GA, USA. [8]Department of Space Physics, Institute of Atmospheric Physics, The Czech Academy of Sciences, Prague, Czechia. [9]Faculty of Mathematics and Physics, Charles University, Prague, Czechia. [10]Department of Physics and Astronomy, University of Iowa, Iowa City, IA, USA. [11]NASA/Goddard Spaceflight Center, Greenbelt, MD, USA. *e-mail: shannon.t.brown@jpl.nasa.gov

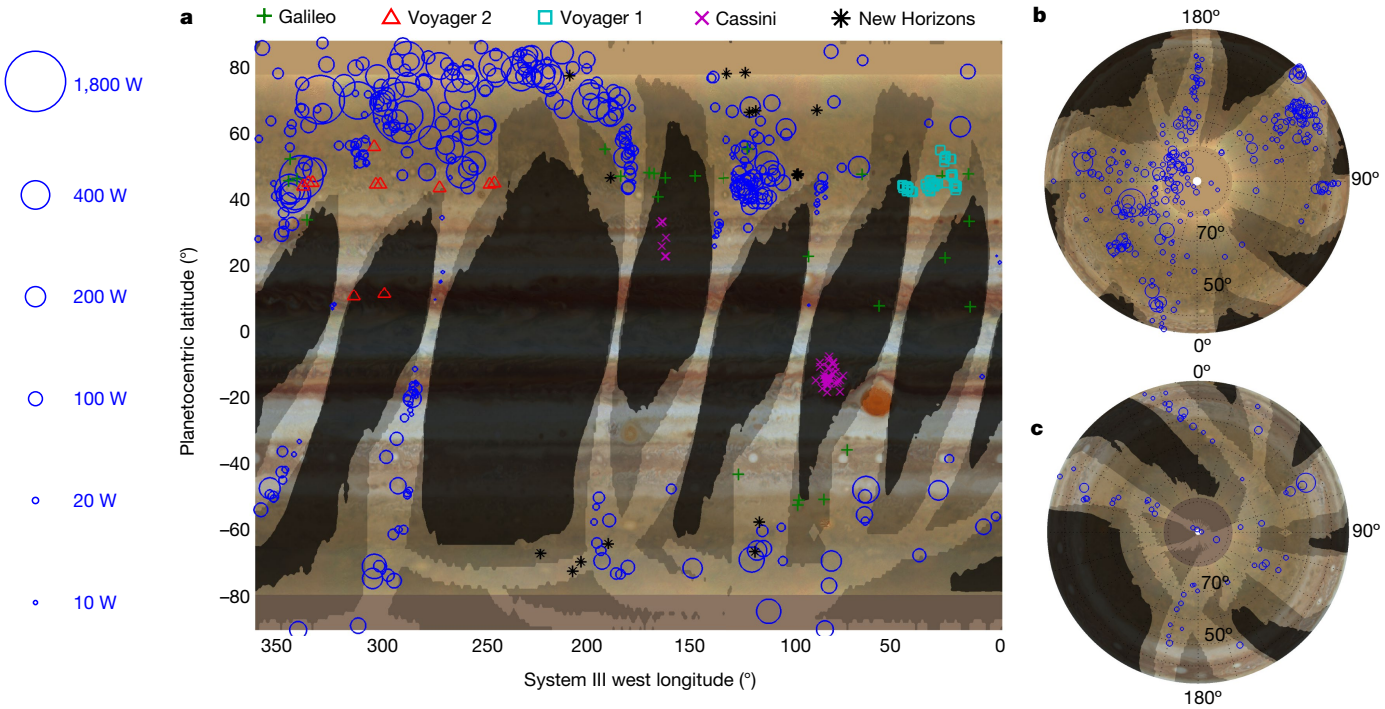

Fig. 1 | MWR boresight location of each 600-MHz lightning detection during Juno's first seven successful passes. Each MWR detection is shown as a blue circle with a diameter proportional to the minimum effective isotropic radiating power (the scale shown on the left corresponds to **a**). **b** and **c** show the north and south polar projection, respectively. The area of the planet surveyed by MWR during each perijove pass is indicated by the bright regions. The brightest regions show the locations of maximum gain and the less bright ones show the area covered by the 3-dB antenna pattern contour. The visible-light background image is aligned with the Great Red Spot overpass, made in July 2017. The other passes are not aligned with visible features in the image because the clouds propagate relative to the System III longitude owing to zonal winds.

excess emission. Similar, but much fewer (12), signatures were detected at 1.2 GHz, and there were no definite detections above 1.2 GHz; this is expected, given the ~f^{-4} dependence of lightning radio emission. The 600-MHz and 1.2-GHz antennas are on different sides of the spacecraft and therefore do not make temporally coincident observations, so a direct measure of the spectral emission slope is not possible. Additional observations are expected to provide statistical constraints, which may provide insight into the nature of the discharge process. The remainder of this paper focuses on the 600-MHz observations.

Figure 1, which illustrates the MWR boresight location and relative strength of each 600-MHz lightning detection, reveals a new and more complete picture of the global lightning distribution. The MWR detections span the locations of previous detections and show lightning polewards of 79° N, the highest latitude reported by New Horizons[6]. Lightning is detected at both poles but is absent near the equator. An additional notable observation is the absence of lightning in the Great Red Spot during the direct Juno overpass on 11 July 2017. The most probable source location of the lightning —the area on the planet that emitted 90% of the power received by the MWR—would fall on average within 10^6 km^2 of the boresight at the equator and 10^9 km^2 at the pole. During the first eight Juno orbits, the antenna footprint (defined by the 3-dB contour) covered 3×10^{10} km^2, or 50% of the planet, in approximately equal amounts between the northern and southern hemispheres. Although uncertainty in the source location does not allow an exact computation of the power transmitted in the direction of the MWR, a lower bound can be computed assuming that the emission is directed at the maximum antenna gain. The derived minimum effective isotropic radiating power for lightning emission spans between 1.2 W and 1,800 W, with 87% of the detections below 200 W and 96% below 400 W. The strongest detections are preferentially weighted towards the northern hemisphere.

We derive the latitude distribution probabilistically, by spreading each detection over a latitude range weighted by the projected antenna gain and normalized by the total observation time per latitude. Figure 2 illustrates that lightning was mostly detected in the northern mid- to high latitudes, revealing an oscillating pattern with peaks near 45° N, 56° N, 68° N and 80° N. There are also peaks centred in the North Equatorial Belt and the North Temperate Belt. The mean probability is higher in the belts (0.0045 detections per

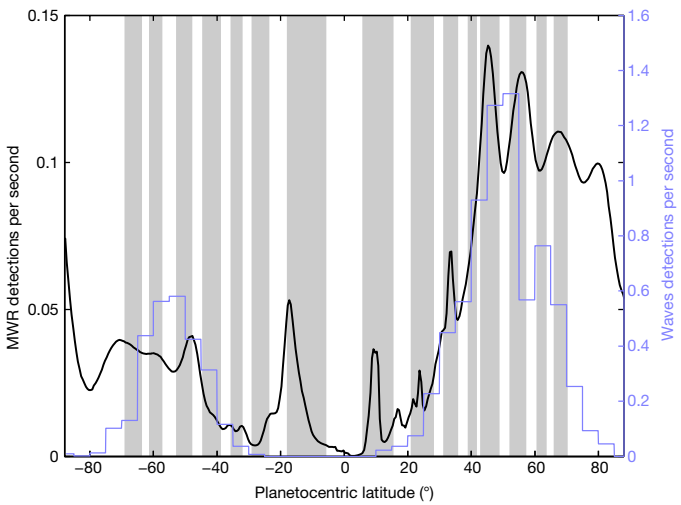

Fig. 2 | Lightning detections per second by the MWR and the Waves instrument as a function of latitude. The black line shows the distribution of sferics observed by the MWR. The lightning detection locations are distributed over the latitude, which is weighted by the projected MWR antenna gain pattern. This accounts for the uncertainty in the lightning source location within the MWR beam in a probabilistic way. The blue line shows the detection frequency of whistlers by the Waves instrument as a function of magnetic footprint latitudes from the VIP4 model. The grey bars indicate the belts with the zones (white bars) in between[30].

second) than in the zones (0.0035 detections per second) for absolute latitudes below 70°. Analysis of Galileo data also found more frequent lightning in belts[4]. In the southern hemisphere, the lightning frequency peaks at 17° S, followed by 48° S. The ambiguity of the lightning source location in the MWR beam gives an effective resolution in latitude (defined by the 3 dB antenna contour averaged over all detections) of about 2° at the equator, 5° at ±45°, and 10° near the poles.

Considerably more lightning is detected in the northern hemisphere than in the southern hemisphere. This hemispherical asymmetry is observed in each perijove pass (spaced every 53 days), so it is not due to a single anomalously active storm in the northern hemisphere. The MWR is closer to the planet, and thus slightly more sensitive to lightning, at a given latitude in the northern hemisphere compared to the southern hemisphere. However, removing those detections in the northern hemisphere that would not have been observed in the southern hemisphere at an equivalent latitude does not affect the observed asymmetry. The equatorial zone is the only place on Jupiter with a near-zero probability of lightning detection. The boresight location of the most equatorial detection is 7.8° N. Accounting for sampling through orbit 8, equatorial lightning (within ±6° of the equator) must occur at a rate of $<0.03\ km^{-2}\ yr^{-1}$ to have a detection probability less than 1 (or be 100 times less intense than lightning at higher latitudes). The absence of lightning at the equator is consistent with the non-detection of lightning at the Galileo probe entry site[12] at 6° N and the absence of visible detections within ±6° of the equator.

Jovian rapid whistlers observed by the Waves instrument[22] show a similar north–south asymmetry, as indicated by the whistler detection frequency per unit time shown in Fig. 2 in 5° latitude bins. The source location of the whistlers is estimated by back-propagation to be 300 km above the 1-bar level along magnetic field lines using the VIP4 model[23]. The overall detection rates of whistlers are approximately ten times higher than the MWR detection rate because of the increased source power at kilohertz frequencies compared to 600 MHz[10]. We note also that whistlers do not show detections within about 20° of the equator, which may be explained by ducted propagation not allowing them to access the Juno altitude. High-latitude observations are mostly missing from whistler records, as these are masked by intense plasma waves in the polar-cap and auroral regions.

The moist convection distribution derived here has implications for the global water abundance and energy budget of Jupiter. While moist convection is a complex process that is influenced in part by the local water concentration, thermodynamic environment and vertical wind shear, the distribution observed here could support a preferentially poleward-weighted distribution of the outward-directed internal heat flux[16,18]. The high concentration of ammonia in the equatorial zone[24,25] suggests that the equator is close to an ideal adiabat[26], potentially explaining the lack of convection at the equator. A rising air parcel in this region would have the same density as the ambient air and would not gain kinetic energy from the upward motion. Moist convection involving water clouds, as inferred from the presence of lightning, provides a constraint on the water abundance. If water were depleted globally below the value of the solar oxygen-to-hydrogen ratio, as would be concluded by taking the Galileo probe result as a global number[27], there would be no liquid water[28] and hence lightning would be difficult to generate[7,8]. Moist convection models also suggest that insufficient latent heat would be available to sustain lightning-generating updrafts[19,20,29]. Previous studies of optical lightning imagery (and the associated moist convection) have used these arguments to suggest a global water abundance greater than the solar one, under the assumption that the convective nature of regional storms observed over a short period of time applies globally and is sustained over time[5,8]. The MWR lightning observations analysed here show widespread moist convective activity at nearly all latitudes consistently for over an Earth year, providing compelling evidence for a global water abundance at least as high as the solar one.

Online content

Any Methods, including any statements of data availability and Nature Research reporting summaries, along with any additional references and Source Data files, are available in the online version of the paper at https://doi.org/10.1038/s41586-018-0156-5.

Received: 21 November 2017; Accepted: 14 March 2018;
Published online 6 June 2018.

1. Gurnett, D. A., Shaw, R. R., Anderson, R. R., Kurth, W. S. & Scarf, F. L. Whistlers 215 observed by Voyager 1: detection of lightning on Jupiter. *Geophys. Res. Lett.* **6**, 511–514 (1979).
2. Cook, A. F., Duxbury, T. C. & Hunt, G. E. First results of Jovian lightning. *Nature* **280**, 794 (1979).
3. Borucki, W. J. & Magalhães, J. A. Analysis of Voyager 2 images of Jovian lightning. *Icarus* **96**, 1–14 (1992).
4. Little, B. et al. Galileo images of lightning on Jupiter. *Icarus* **142**, 306–323 (1999).
5. Dyudina, U. A. et al. Lightning on Jupiter observed in the Hα line by the Cassini imaging science subsystem. *Icarus* **172**, 24–36 (2004).
6. Baines, K. H. et al. Polar lightning and decadal-scale cloud variability on Jupiter. *Science* **318**, 226–229 (2007).
7. Rinnert, K. Lightning on other planets. *J. Geophys. Res. D* **90**, 6225–6237 (1985).
8. Gibbard, S., Levy, E. H. & Lunine, J. I. Generation of lightning in Jupiter's water cloud. *Nature* **378**, 592–595 (1995).
9. Gierasch, P. J., Ingersoll, A. P., Banfield, D. & Ewald, S. P. Observation of moist convection in Jupiter's atmosphere. *Nature* **403**, 628–630 (2000).
10. Oh, L. L. Measured and calculated spectral amplitude distribution of lightning sferics. *IEEE Trans. Electromagn. Compat.* **4**, 125–130 (1969).
11. LeVine, D. M. & Meneghini, R. Simulation of radiation from lightning return strokes: the effects of tortuosity. *Radio Sci.* **13**, 801–809 (1978).
12. Rinnert, K. et al. Measurements of radio frequency signals from lightning in Jupiter's atmosphere. *J. Geophys. Res. Planets* **103**, 22979–22992 (1998).
13. Farrell, W. M. in *Radio Astronomy at Long Wavelengths* (eds Stone, R. G. et al.) 179–186 (American Geophysical Union, Washington DC, 2000).
14. Zarka, P. On detection of radio bursts associated with Jovian and Saturnian lightning. *Astron. Astrophys.* **146**, L15–L18 (1985).
15. Janssen, M. A. et al. MWR: microwave radiometer for the Juno mission to Jupiter. *Space Sci. Rev.* **213**, 139–185 (2017).
16. Ingersoll, A. P. & Porco, C. C. Solar heating and internal heat flow on Jupiter. *Icarus* **35**, 27–43 (1978).
17. Ingersoll, A. P., Gierasch, P. J., Banfield, D., Vasavada, A. R. & Galileo Imaging Team. Moist convection as an energy source for the large-scale motions in Jupiter's atmosphere. *Nature* **403**, 630–632 (2000).
18. Pirraglia, J. A. Meridional energy balance of Jupiter. *Icarus* **59**, 169–176 (1984).
19. Stoker, C. R. Moist convection: a mechanism for producing the vertical structure of the Jovian equatorial plumes. *Icarus* **67**, 106–125 (1986).
20. Guillot, T. Condensation of methane, ammonia, and water and the inhibition of convection in giant planets. *Science* **269**, 1697–1699 (1995).
21. Majeed, T., McConnell, J. C. & Gladstone, G. R. A model analysis of Galileo electron densities on Jupiter. *Geophys. Res. Lett.* **26**, 2335–2338 (1999).
22. Kolmašová, I. et al. Discovery of rapid whistlers close to Jupiter implying similar lightning rates as on Earth. *Nat. Astron.* https://doi.org/10.1038/s41550-018-0442-z (2018).
23. Connerney, J. E. P., Acuña, M. H., Ness, N. F. & Satoh, T. New models of Jupiter's magnetic field constrained by the Io flux tube footprint. *J. Geophys. Res.* **103**, 11929–11939 (1998).
24. Bolton, S. J. et al. Jupiter's interior and deep atmosphere: the initial pole-to-pole passes with the Juno spacecraft. *Science* **356**, 821–825 (2017).
25. Li, C. et al. The distribution of ammonia on Jupiter from a preliminary inversion of Juno Microwave Radiometer data. Geophys. *Res. Lett.* **44**, 5317–5325 (2017).
26. Ingersoll, A. P. et al. Implications of the ammonia distribution on Jupiter from 1 to 100 bars as measured by the Juno microwave radiometer. *Geophys. Res. Lett.* **44**, 7676–7685 (2017).
27. Niemann, H. B. et al. The composition of the Jovian atmosphere as determined by the Galileo probe mass spectrometer. *J. Geophys. Res. Planets* **103**, 22831–22845 (1998).
28. Atreya, S. K. et al. Comparison of the atmospheres of Jupiter and Saturn: deep atmospheric composition, cloud structure, vertical mixing, and origin. *Planet. Space Sci.* **47**, 1243–1262 (1999).
29. Hueso, R. & Sánchez-Lavega, A. A three-dimensional model of moist convection for the giant planets: the Jupiter case. *Icarus* **151**, 257–274 (2001).
30. Porco, C. C. et al. Cassini imaging of Jupiter's atmosphere, satellites, and rings. *Science* **299**, 1541–1547 (2003).

Acknowledgements This research was carried out at the Jet Propulsion Laboratory, California Institute of Technology, under a contract with the National Aeronautics and Space Administration. The research at the University of Iowa was supported by NASA through contract 699041X with the Southwest Research Institute. The work of I.K. and O.S. was supported by grants MSM100421701 and LTAUSA17070 and by the Praemium Academiae award.

Reviewer information *Nature* thanks U. Dyudina and the other anonymous reviewer(s) for their contribution to the peer review of this work.

Author contributions S. Br. analysed the MWR data to find and extract the lightning observations. M.J. is the co-investigator lead of the MWR. S.A., A.I., C.L., J.L., L.L., G.O., P.S., S. Bo. and F.T.-V. contributed to the interpretation of the data and the implications for atmospheric processes. S.G., S.M. and V.A. contributed to the interpretation of the radiometric source signal. I.K., M.I. and O.S. calculated whistler rates. W.S.K., G.B.H. and D.A.G advised on data analysis. W.S.K. is responsible for the Juno Waves instrument. J.E.P.C. provided the planetary magnetic field measurements. S. Br. wrote the manuscript with input from all authors.

Competing interests The authors declare no competing interests.

Additional information
Extended data is available for this paper at https://doi.org/10.1038/s41586-018-0156-5.
Reprints and permissions information is available at http://www.nature.com/reprints.
Correspondence and requests for materials should be addressed to S.Br.
Publisher's note: Springer Nature remains neutral with regard to jurisdictional claims in published maps and institutional affiliations.

METHODS

Lightning detection methodology. In the MWR data, lightning is observed as single positive outliers in the time series of the antenna temperature. The MWR integrates each sample for 0.1 s, during which time the spacecraft rotates by 1.2°, or about 1/17th of an antenna beamwidth at 600 MHz and 1.2 GHz. This means that each sample is correlated with its neighbours, and only a short (<0.1 s) radio-frequency impulse on top of the background brightness temperature distribution could produce such a discrete jump in the time series. Instrument anomalies were eliminated as the source of these outliers by evaluating high-rate data during the cruise portion of the mission and several high-rate acquisitions near apojove. No outliers greater than four standard deviations above the noise were observed in approximately 5,000 h of observations through the antenna or in the accompanying observations of internal calibration sources. During the perijove pass, outliers were observed only when the radiometer was pointed towards the planet, and not away from the planet, eliminating radiation effects or other anomalies unique to the Jovian environment as the cause. The most probable source of short radio-frequency emission bursts from Jupiter is thus lightning.

Extended Data Fig. 1 shows an example of a lightning detection. The left panel shows the antenna temperature time series from approximately one spin of the spacecraft. The centre of the plot shows the scan across Jupiter, with the peak value closest to nadir. The large lobes on either side of the planet near the limb arise from synchrotron radiation. The cold sky background forms the baseline level. The lightning observation is the single-point outlier on the planet, which is shown more clearly in the zoomed-in image in the right panel.

The outliers are extracted from the time series using a two-step process. First, the data are low-pass-filtered using a 15-point local least-squares regression smoothing method. Positive outliers in the difference between the measurements and the smoothed background that are greater than 5 K (six standard deviations above the noise floor) are identified and removed. Linear interpolation is used to fill in the gaps from the filtered outliers and a second low-pass filter is applied to this 'cleaned' time series to estimate the background antenna temperature as a function of time. Extended Data Fig. 2a shows 600-MHz antenna temperatures obtained during a single Juno spin, with the smoothed background antenna temperature overlaid. The lightning observation in this case is the red outlier point. The final step subtracts the measurements from the smoothed background antenna temperature and all positive outliers greater than 5 K are extracted as lightning observations. An example of this difference for perijove 7 is shown in Extended Data Fig. 2b. The noise on this difference is a combination of instrument noise (∼0.6 K) and noise from the background removal. The noise (excluding the positive outliers) is consistent with a zero mean Gaussian distribution with a standard deviation of 0.8 K. The 5 K detection threshold is set conservatively to minimize the number of false positives. Extended Data Fig. 2c shows the difference between the antenna temperature and the background for all perijove passes through orbit 7. The negative-temperature part of the histogram guided the choice for the 5 K threshold, which is indicated by the vertical dashed lines in the figure.

Analysis of detection biases. To assess the statistical robustness of these conclusions, we must understand possible detection biases in the data. The 5 K detection threshold in the antenna temperature is based on received power, which introduces a sampling bias relative to source emission that varies with the square of the distance to the planet (R^2). The MWR is approximately 100 times more sensitive to a single lightning flash at perijove (a few degrees north of the equator) than it is as the pole. However, the received power is the sum of all lightning flashes in a single sample, and polar observations cover 30–40 times more area on the planet than those made at the equator. Therefore, the lightning detectability in the MWR ultimately depends on how close the average transmission strength is to the threshold at a given distance and spatial density of lightning, both of which are unknown.

If we assume that lightning is sufficiently sparse so that each MWR detection originates from a single source, the difference in area from each observation is not a factor. We can therefore normalize the power received during each observation to the perijove by scaling by the square of the ratio of the observation distance to the perijove distance, as shown in Extended Data Fig. 3a. The minimum detection threshold, shown as the solid black line, varies with R^2 and is slightly skewed towards the northern hemisphere because Juno's perijoves are all north of the equator. The dashed red line represents a detection threshold that is symmetric about the equator. Even if we removed the northern hemisphere observations that would not be detectable in the southern hemisphere at an equivalent latitude, there would still be more numerous and stronger detections in the northern hemisphere. We can also compute an upper limit on the lightning rate at the equator. The MWR acquired 5,690 samples within ±6° of the equator through perijove 8. On average, each sample is integrated over an effective area of 2×10^6 km^2 for 0.1 s. Therefore, for the probability of detection to be less than 1, the lightning flash rate within ±6° must be less than 0.03 km^{-2} yr^{-1}, $\frac{1}{(2\times10^6\,\mathrm{km}^2)\,(569\,\mathrm{s})}$ 31, 557, 600 s yr^{-1}, or be 100 times less intense than lightning at higher latitudes.

Alternatively, if we assume lightning is sufficiently dense so that the number of transmitters that are visible per observation is proportional to the area, then it is appropriate to scale the received power by the area illuminated. The signal received by the MWR from lightning is the integral of all discharges occurring in the area of the planet that is illuminated by the antenna over the 0.1 s integration period. The power at the receiver is a function of the spacecraft location and viewing angle relative to the planet. To allow comparisons between different locations on the planet, we normalize the measurements with respect to source power. However, without knowing the source location, we cannot determine the source power from the received signal. We can compute a power density to normalize the measurements. If we assume that lightning radiates isotropically with a power of P_{iso} and has a discharge frequency of N_{l} per unit area of the planet per unit time, then we can write the total received power as

$$P_{\mathrm{r}} = \iint \frac{N_{\mathrm{l}} P_{\mathrm{iso}} G(\boldsymbol{r}_{\mathrm{dA}})\lambda^2}{(4\pi)^2 |\boldsymbol{r}_{\mathrm{dA}}|^2} \mathrm{d}A\mathrm{d}t \tag{1}$$

where $\boldsymbol{r}_{\mathrm{dA}}$ is the vector between the differential area of the planet, dA, and the MWR antenna, G is the antenna gain in that direction, λ is the wavelength and t is the time. We can use equation (1) to normalize the received power measurements

$$N_{\mathrm{l}} P_{\mathrm{iso}} = \frac{P_{\mathrm{r}}}{\iint \frac{G(\boldsymbol{r}_{\mathrm{dA}})\lambda^2}{(4\pi)^2 |\boldsymbol{r}_{\mathrm{dA}}|^2} \mathrm{d}A\mathrm{d}t} \tag{2}$$

where $N_{\mathrm{l}} P_{\mathrm{iso}}$ is the received isotropic radiated power per unit area per unit time (W km^{-2} s^{-1}).

Extended Data Fig. 3b shows the lightning power normalized using equation (2). The minimum detection threshold in this case is more uniform in latitude because the illumination area increases as R^2, offsetting the decrease in signal strength with distance. In both cases, the larger number of observations in the northern hemisphere appears to be a statistically robust conclusion. Removing from the northern-hemisphere data those values that would not be detected in the southern hemisphere at an equivalent latitude gives the red line in Extended Data Fig. 4; there is negligible change in the resulting north–south asymmetry.

Effective isotropic radiating power. The received power is computed from the lightning antenna temperature by

$$P_{\mathrm{r}} = kBT_{\mathrm{A}} \tag{3}$$

where the 600-MHz receiver bandwidth is $B = 18$ MHz and k is Boltzmann's constant. Because the MWR measures a single linear polarization, if lightning emission is assumed to be unpolarized, a factor of 2 is introduced between the received and source power. The effective isotropic radiating power is then computed by

$$P_{\mathrm{iso}} = \frac{2P_{\mathrm{r}}(4\pi R)^2}{G_{\mathrm{r}}\lambda^2} \tag{4}$$

where R is taken to be the distance of the boresight vector to Jupiter, G_{r} is the maximum antenna gain (19.77 dB) and the wavelength λ is 0.5 m. The result represents the minimum radiated power and only applies when the boresight is pointed directly at the lightning. The lightning is probably detected over a broad range of angles (and hence antenna gains) relative to the boresight.

Data availability. The Juno MWR data that support the findings of this study are available from the Planetary Data System archive (https://pds.nasa.gov/index.shtml) as 'Juno Jupiter MWR reduced data records v1.0' (dataset JNO-J-MWR-3-RDR-V1.0).

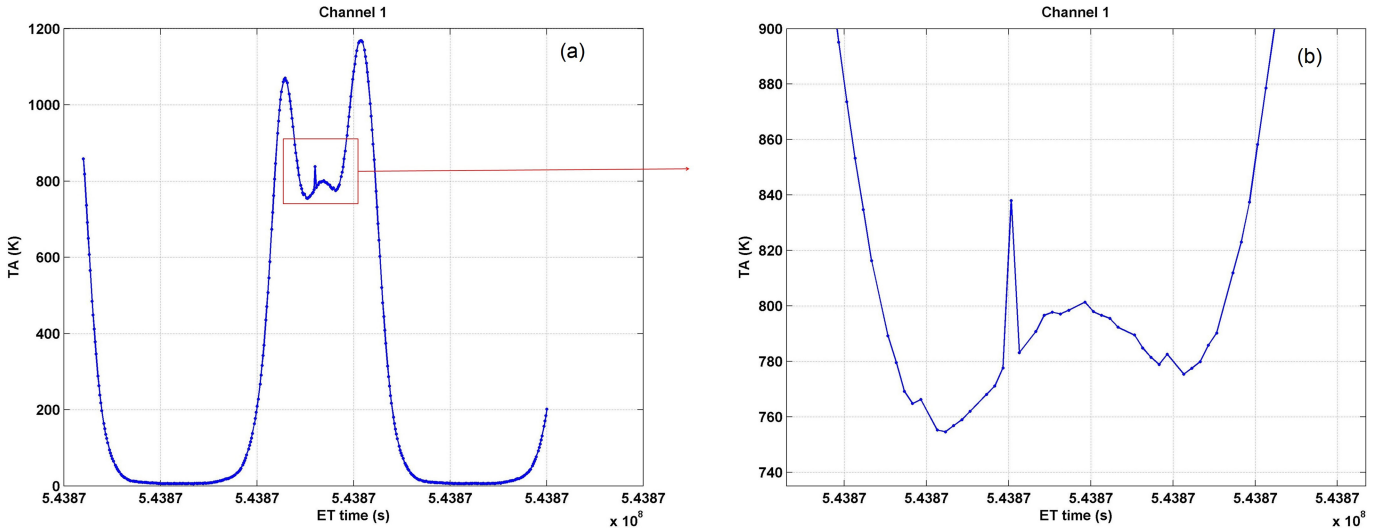

Extended Data Fig. 1 | Example of lightning detection in the MWR antenna temperature time series. a, Antenna temperature measurements obtained during a spin of the spacecraft. The scan from limb to limb of Jupiter is shown at the centre of the image and enlarged in panel **b**. The single positive outlier is the additive emission from the lightning discharge above the background emission from the atmosphere.

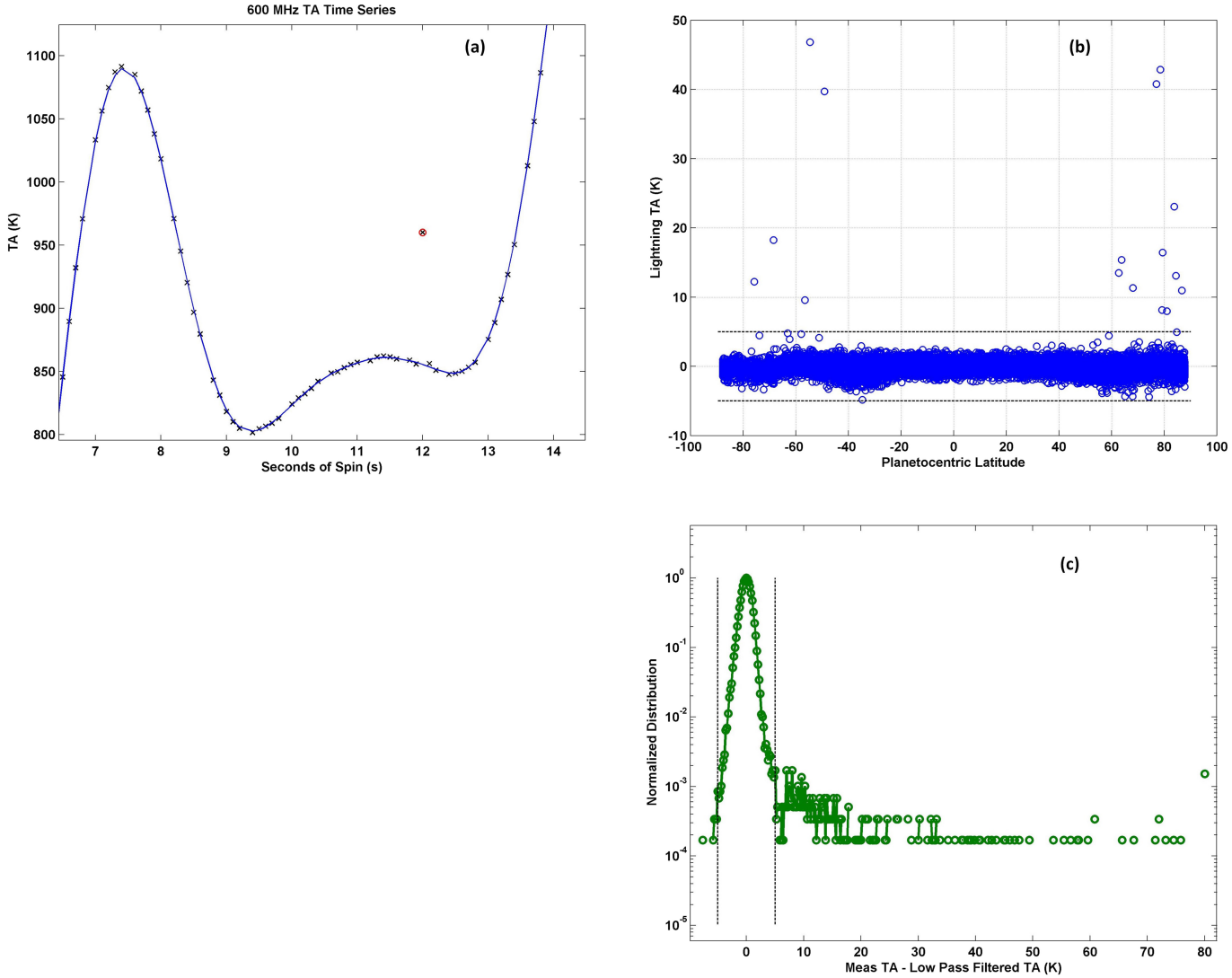

Extended Data Fig. 2 | Illustration of the lightning extraction process. **a**, Smoothed background antenna temperature (TA) and the data. **b**, Difference between the measurements and the smoothed background antenna temperature for perijove 7. **c**, Differences between the MWR data and the background antenna temperature for all perijoves. The dotted lines in **b** and **c** indicate where the detection threshold is set relative to the variance in the data.

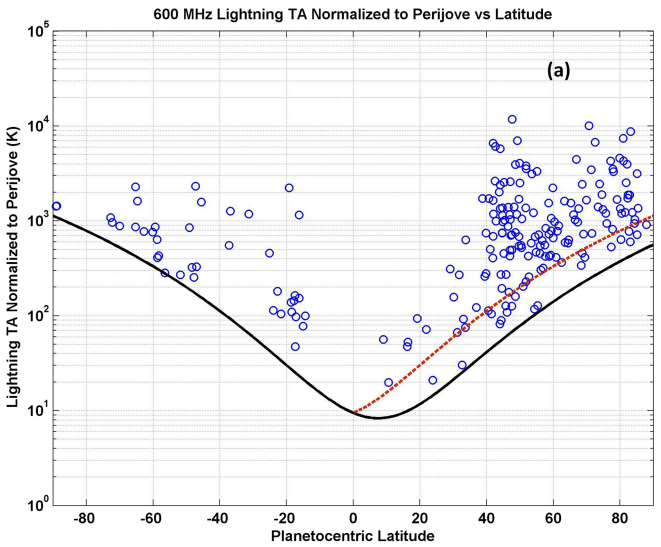

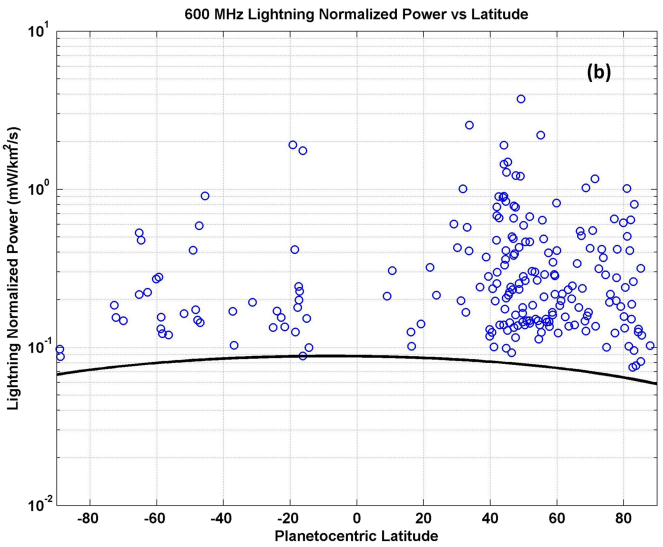

Extended Data Fig. 3 | Normalized 600-MHz lightning power, expressed as antenna temperature, as a function of latitude. a, Power normalized to the perijove distance by the square of the distance. This normalization is used if the observed power from each detection originates from a single source, which is expected for discharge rates less than 300 km^{-2} yr^{-1} near the equator and 0.3 km^{-2} yr^{-1} at the poles. **b**, Power normalized by both the distance and the area covered by the antenna pattern, which is used if the observed power originates from several sources and should be scaled per unit area.

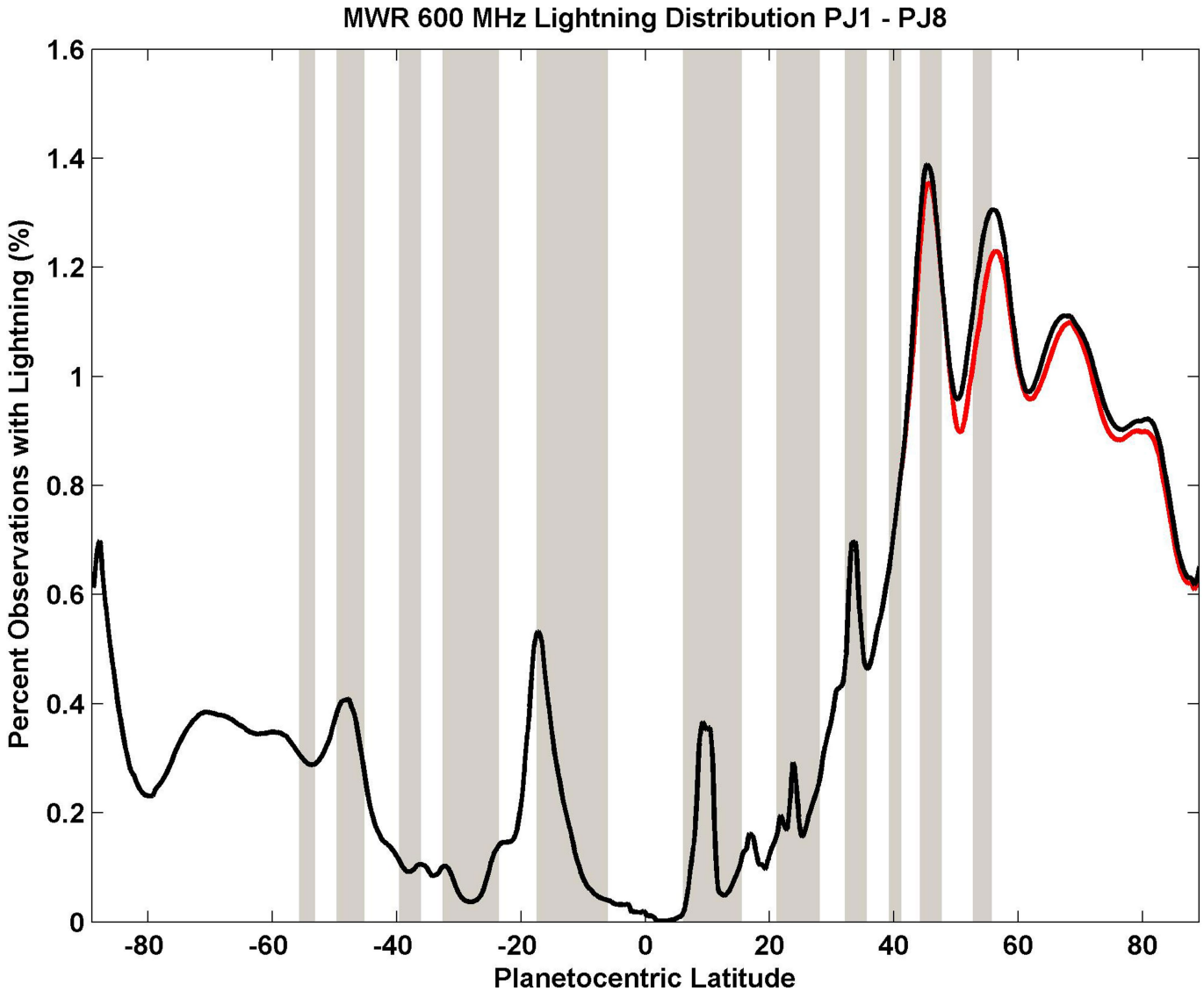

Extended Data Fig. 4 | Lightning detections per second by the MWR and the Waves instrument as a function of latitude. The same MWR distribution as that shown in Fig. 2, but with the red line showing the distribution with an equalized detection threshold as a function of latitude.